PHYSICAL REVIEW D **91,** 075002 (2015)

LHC searches for the *CP*-odd Higgs boson with a jet substructure analysis

Ning Chen,[1,*] Jinmian Li,[2,†] Yandong Liu,[3,‡] and Zuowei Liu[4,§]

[1]*Department of Modern Physics, University of Science and Technology of China, Hefei, Anhui 230026, China*

[2]*ARC Centre of Excellence for Particle Physics at the Terascale, School of Chemistry and Physics, University of Adelaide, Adelaide, South Australia 5005, Australia*

[3]*Department of Physics and State Key Laboratory of Nuclear Physics and Technology, Peking University, Beijing 100871, China*

[4]*Center for High Energy Physics, Tsinghua University, Beijing 100084, China*

(Received 29 October 2014; published 7 April 2015)

The LHC searches for the *CP*-odd Higgs boson A are studied (with masses from 300 GeV to 1 TeV) in the context of the general two-Higgs-doublet model. With the discovery of the 125 GeV Higgs boson at the LHC, we highlight one promising discovery channel of $A \to hZ$. This channel can become significant for a heavy *CP*-odd Higgs boson after the global signal fitting to the 125 GeV Higgs boson in the general two-Higgs-doublet model. It is particularly interesting in the scenario where two *CP*-even Higgs bosons in the two-Higgs-doublet model have the common mass of 125 GeV. Since the final states involve a standard-model-like Higgs boson, we apply the jet substructure analysis of tagging the fat Higgs jet in order to eliminate the standard-model background sufficiently. After performing the kinematic cuts, we present the LHC search sensitivities for the *CP*-odd Higgs boson with mass up to 1 TeV via this channel.

DOI: 10.1103/PhysRevD.91.075002 PACS numbers: 12.60.Fr, 14.80.-j, 14.80.Ec

I. INTRODUCTION

The study of the Higgs mechanism [1–3] has become more interesting and important since the discovery of the 125 GeV Higgs boson at the LHC $7 \oplus 8$ TeV runs. The properties of the 125 GeV Higgs boson, such as the coupling strengths with standard-model (SM) fermions and gauge bosons [4], its spin and parity [5], and the exotic decay channels [6], will be further measured in the next LHC runs and the future high-energy colliders. From various motivations, the SM Higgs mechanism is far from being complete. New physics models beyond the SM are proposed to address different questions, which typically contain new states in the spectrum. In many of them, the electroweak symmetry breaking is due to the extended Higgs sector. Examples include the minimal supersymmetric extension of the SM [7], the twin Higgs models [8], and the composite Higgs models [9]. The future experimental searches for the new degrees of freedom in the spectra provide direct avenues for revealing the new physics underneath.

A very widely studied scenario beyond the minimal one-doublet setup is the two-Higgs-doublet model (2HDM), which is the low-energy description of the scalar sectors in many new physics models. A recent review of the phenomenology in the context of the general 2HDM can be found in Ref. [10]. References [11–27] studied the 2HDM phenomenology at the LHC in light of the Higgs discovery. The scalar spectrum in the 2HDM contains five states, namely, two neutral *CP*-even Higgs bosons (h, H), one neutral *CP*-odd Higgs boson A, and two charged Higgs bosons $H^{\pm}$. Often, one would interpret the lighter *CP*-even Higgs boson h as the one discovered at the LHC. In the context of the general 2HDM, each Higgs boson mass is actually a free parameter before applying any constraint. A special parameter set in the general 2HDM is when two *CP*-even Higgs bosons (h, H) are degenerate in mass. The diphoton signal predictions with this special parameter choice in the 2HDM scenario were studied in Ref. [14].

Within the framework of the 2HDM, we study the future LHC searches for the *CP*-odd Higgs boson A at the 14 TeV run. The previous experimental searches often focus on the benchmark models in the minimal supersymmetric standard model, which has type-II 2HDM Yukawa couplings. Thus, the interesting final states to be looked for are the $A \to \bar{b}b$ [28,29] and $A \to \tau^+\tau^-$ [30–36] since the relevant Yukawa couplings are likely to be significantly enhanced. Different from the existing experimental search modes, we focus on the decay channel of $A \to hZ$. The previous studies to this search channel at the LHC include Refs. [13,15,19], where the final states of $\bar{b}b\ell^+\ell^-$, $\tau^+\tau^-\ell^+\ell^-$, and ZZZ were studied. Also, an experimental analysis of this search channel with multiple lepton and photon final states was carried out at the LHC 8 TeV run [37]. Here, in our analysis, we will focus on the $\bar{b}b\ell^+\ell^-$ final state coming from the decay channel of $A \to hZ$. In this case, the final states involve a SM-like Higgs boson

*chenning@ustc.edu.cn
†jinmian.li@adelaide.edu.au
‡ydliu@pku.edu.cn
§zuoweiliu@tsinghua.edu.cn

with mass of 125 GeV. Therefore, the jet substructure method of tagging the boosted Higgs jet can be potentially instrumental for this particular channel in our study. The method of tagging the boosted Higgs jets was suggested in Refs. [38,39], in which the discovery potential of the SM Higgs boson via the hV-associated production channel at the LHC was investigated. Later, this procedure was widely adopted in searches for new resonances with a SM-like Higgs boson as their decay final states [39–42] and in studies of the SM-like Higgs boson properties at the LHC [43–45].

This paper is organized as follows. In Sec. II, we give a brief review on the CP-odd Higgs boson A in the context of the general 2HDM. We list its coupling terms, with the emphasis on the derivative couplings of AhZ and AHZ. In Sec. III, we evaluate the productions and decays of the CP-odd Higgs boson A in the context of the general 2HDM. We show that the decay mode of $A \to hZ$ can be sizable for the future LHC searches at the 14 TeV runs, given the current global fit to the 2HDM parameters. We also show that for the degenerate Higgs scenario of $M_h = M_H = 125$ GeV, the decay modes of $A \to hZ/HZ$ are typically dominant over all other decay modes into the SM final states. Hence, such a mode can be regarded as the leading one for the future searches for the CP-odd Higgs boson in this special case. In Sec. IV, the analysis of LHC searches for the CP-odd Higgs boson via the $A \to hZ$ final states is provided. In order to eliminate the SM background sufficiently, we apply the jet substructure method developed in Ref. [38] to tag the fat Higgs jet directly with the Cambridge-Aachen (CA) jet algorithm [46,47]. Optimizations to the jet substructure methods and kinematic cuts for the signal processes are presented. The LHC search potential to the $A \to hZ$ decay channel at different phases of the upcoming runs at 14 TeV is also shown. The conclusions are given in Sec. V.

II. *CP*-ODD HIGGS BOSON IN THE 2HDM

A. *CP*-odd Higgs boson mass

The most general 2HDM Higgs potential that is CP conserving contains three mass terms plus seven more quartic coupling terms. For simplicity, we consider the soft breaking of a discrete $\mathbb{Z}_2$ symmetry, under which the two Higgs doublets transform as $(\Phi_1, \Phi_2) \to (\Phi_1, -\Phi_2)$. The simplified 2HDM potential is expressed as

$$\begin{aligned} V(\Phi_1,\Phi_2) = {} & m_{11}^2|\Phi_1|^2 + m_{22}^2|\Phi_2|^2 - m_{12}^2(\Phi_1^\dagger\Phi_2 + \text{H.c.}) \\ & + \frac{1}{2}\lambda_1|\Phi_1|^4 + \frac{1}{2}\lambda_2|\Phi_2|^4 + \lambda_3|\Phi_1|^2|\Phi_2|^2 \\ & + \lambda_4|\Phi_1^\dagger\Phi_2|^2 + \frac{1}{2}\lambda_5[(\Phi_1^\dagger\Phi_2)(\Phi_1^\dagger\Phi_2) + \text{H.c.}], \end{aligned} \tag{1}$$

where all parameters are real. The two Higgs doublets Φ_1 and Φ_2 pick up vacuum expectation values to trigger the electroweak symmetry breaking

$$\langle\Phi_1\rangle = \frac{1}{\sqrt{2}}\begin{pmatrix} 0 \\ v_1 \end{pmatrix}, \qquad \langle\Phi_2\rangle = \frac{1}{\sqrt{2}}\begin{pmatrix} 0 \\ v_2 \end{pmatrix}, \tag{2}$$

and one often parametrizes the ratio of the two Higgs vacuum expectation values as

$$t_\beta \equiv \tan\beta \equiv \frac{v_2}{v_1}. \tag{3}$$

Expressing the two Higgs doublets in components, we have

$$\Phi_i = \begin{pmatrix} \pi_i^+ \\ (v_i + h_i + i\pi_i^0)/\sqrt{2} \end{pmatrix}, \qquad i = 1, 2. \tag{4}$$

Three of the eight components are Nambu-Goldstone bosons giving rise to the electroweak gauge boson masses, with the remaining five components as the physical Higgs bosons: two CP-even Higgs bosons h and H, one CP-odd Higgs boson A, and the charged Higgs bosons $H^\pm$. The CP-odd Higgs boson A is a linear combination of the two imaginary components π_i^0 in the doublets: $A = -s_\beta\pi_1^0 + c_\beta\pi_2^0$, whereas the orthogonal linear combination of $G = c_\beta\pi_1^0 + s_\beta\pi_2^0$ corresponds to the Nambu-Goldstone mode to be eaten by the Z boson. By extracting the relevant terms in the 2HDM potential (1), the CP-odd Higgs boson mass square is given by

$$M_A^2 = (m_{12}^2 - \lambda_5 v_1 v_2)(t_\beta + 1/t_\beta). \tag{5}$$

B. Couplings of the *CP*-odd Higgs boson

In the context of the general 2HDM, one usually couples fermions with the same quantum numbers to the same Higgs doublet, which will avoid the tree-level flavor-changing neutral currents. In the 2HDM-I, all SM fermions couple to one Higgs doublet (conventionally chosen to be Φ_2). In the 2HDM-II, the up-type quarks u_i couple to one Higgs doublet (conventionally chosen to be Φ_2) and the down-type quarks d_i and the charged leptons ℓ_i couple to the other (Φ_1). Details of the Yukawa setups in the 2HDM-I and 2HDM-II can be found in Ref. [10]. At the tree level, the CP-odd Higgs boson A couples to the SM fermions through the Yukawa coupling terms

$$-\mathcal{L}_Y^A = -i\sum_f \frac{m_f}{v}\xi_A^f \bar{f}\gamma_5 f A, \tag{6}$$

where f is the SM fermion, m_f is the SM fermion mass, and $v = \sqrt{v_1^2 + v_2^2} = (\sqrt{2}G_F)^{-1/2} = 246$ GeV. The relevant coupling strengths of ξ_A^f are listed in Table I for the

2HDM-I and 2HDM-II cases. The loop-induced couplings such as Agg and $A\gamma\gamma$ are also correlated with the Yukawa coupling strengths of ξ_A^f. In addition, there are relevant derivative couplings of the CP-odd Higgs boson A with the Z boson and the CP-even Higgs bosons (h, H), which arise from the kinematic terms of $|D\Phi_i|^2$. The couplings of AhZ and AHZ read

$$\sim\frac{1}{2}(gW^3 - g_Y B)\cdot[h_i(\partial\pi_i^0) - \pi_i^0(\partial h_i)]$$
$$\Rightarrow \frac{g}{2c_W}Z\cdot\{c_{\alpha-\beta}[h(\partial A) - A(\partial h)] + s_{\alpha-\beta}[H(\partial A) - A(\partial H)]\}, \tag{7}$$

where we express them in terms of the mass eigenstates $c_{\alpha-\beta}\equiv\cos(\alpha-\beta)$ and $s_{\alpha-\beta}\equiv\sin(\alpha-\beta)$. Here α represents the mixing angle of the CP-even Higgs bosons. In many cases, one would regard the lighter CP-even Higgs boson h as the 125 GeV Higgs boson discovered at the LHC, while others are regarded as heavier scalars to be searched for in the upcoming LHC runs. In the context of the general 2HDM, we also consider the degenerate Higgs scenario with $M_h = M_H = 125$ GeV. The CP-odd Higgs boson A can also decay to the final states of $H^\pm W^\mp$ due to the derivative coupling terms of $AH^\pm W^\mp$ in the 2HDM kinematic terms. In our study here, we will always take the heavy mass input for $M_{H^\pm}$ and the decay modes of $A\to H^\pm W^\mp$ will not be addressed. The search for this decay mode was recently studied in Ref. [25].

At the end of this section, we mention the constraints on the 2HDM parameters in light of the 125 GeV Higgs boson discovery at the LHC. In studies of the 2HDM, it is often assumed that the lightest CP-even Higgs boson h in the spectrum corresponds to the 125 GeV Higgs boson discovered at the LHC $7\oplus 8$ TeV runs. Under this assumption, one can perform a global fit to the signal strengths of h based on a particular 2HDM setup. Only two parameters (α,β) are relevant for determining the gauge couplings of g_{hVV} and the Yukawa couplings of g_{hff}. Details of such global fits can be found in Refs. [14,48]. Given that the current signals in various decay channels are generally close to the SM Higgs boson predictions, the global fits to the allowed 2HDM parameter regions on (α,β) are consistent with the so-called "alignment limit" where $c_{\beta-\alpha}\to 0$. Consequently, one has $g_{hVV}\to g_{hVV}^{(\mathrm{SM})}$ and $g_{hff}\to g_{hff}^{(\mathrm{SM})}$ in this limit. Because of different Yukawa coupling patterns, the allowed regions of $c_{\beta-\alpha}$ are typically $\sim\mathcal{O}(0.1)$ for the 2HDM-I case, and are more stringently constrained to be $\sim\mathcal{O}(0.01)$ in the 2HDM-II case. In the analysis below, we take the following alignment parameter sets

$$\text{2HDM-I: } c_{\beta-\alpha}=0.2, \quad \text{2HDM-II: } c_{\beta-\alpha}=-0.02, \tag{8}$$

when we take h to be the only state with mass of 125 GeV. Since the relevant coupling terms given in Eq. (7) depend on the angle $\alpha-\beta$, this suggests the partial width of $\Gamma[A\to hZ]$ is suppressed due to the smallness of $c_{\beta-\alpha}$. However, for the larger M_A region, this decay mode is likely to dominate over the fermionic decay modes, such as $A\to\bar{t}t$. Besides, we shall also consider the degenerate Higgs scenario with $M_h = M_H = 125$ GeV in the 2HDM spectrum, where one cannot distinguish the decay modes of $A\to hZ$ and $A\to HZ$. Under this case, the combined decay widths of $\Gamma[A\to h/H+Z]$ should be considered for the LHC analysis, which is no longer suppressed by the small $c_{\alpha-\beta}$ parameter, and thus the partial decay widths of $\Gamma[A\to h/H+Z]$ are generally dominant over all others for the CP-odd Higgs boson. In what follows, we will always use $A\to hZ$ for both the $M_h = 125$ GeV scenario and the $M_h = M_H = 125$ GeV scenario.

III. PRODUCTIONS AND DECAYS OF THE *CP*-ODD HIGGS BOSON *A*

A. Productions of *A*

The CP-odd Higgs boson A can be produced from both the gluon fusion and the bottom-quark annihilation processes [49,50]. The relevant Feynman diagrams for these processes are depicted in Fig. 1. At leading order, the partonic production cross section of $\hat{\sigma}(gg\to A)$ is related to the gluonic partial decay width as follows

$$\hat{\sigma}(gg\to A) = \frac{\pi^2}{8M_A}\Gamma[A\to gg]\delta(\hat{s}-M_A^2), \tag{9a}$$

$$\Gamma[A\to gg] = \frac{G_F\alpha_s^2 M_A^3}{64\sqrt{2}\pi^3}\left|\sum_q \xi_A^q A_{1/2}^A(\tau_q)\right|^2, \tag{9b}$$

with $\tau_q\equiv M_A^2/(4m_q^2)$ and ξ_A^q being the Yukawa couplings given in Table I. Here $A_{1/2}^A(\tau)$ is the fermionic loop factor for the pseudoscalar. In the heavy quark mass limit of $m_q\gg M_A$, this loop factor reaches the asymptotic value of $A_{1/2}^A(\tau)\to 2$, while it approaches 0 in the chiral limit of $m_q\ll M_A$. For the 2HDM-I case, the dominant contribution to the gluon fusion process is always the top-quark loop; for the 2HDM-II case, however, the contribution from the bottom-quark loop can become comparable to the

TABLE I. The Yukawa couplings of the SM quarks and charged leptons to the CP-odd Higgs boson A in the 2HDM-I and 2HDM-II.

	2HDM-I	2HDM-II
ξ_A^u	$1/t_\beta$	$1/t_\beta$
ξ_A^d	$-1/t_\beta$	t_β
ξ_A^ℓ	$-1/t_\beta$	t_β

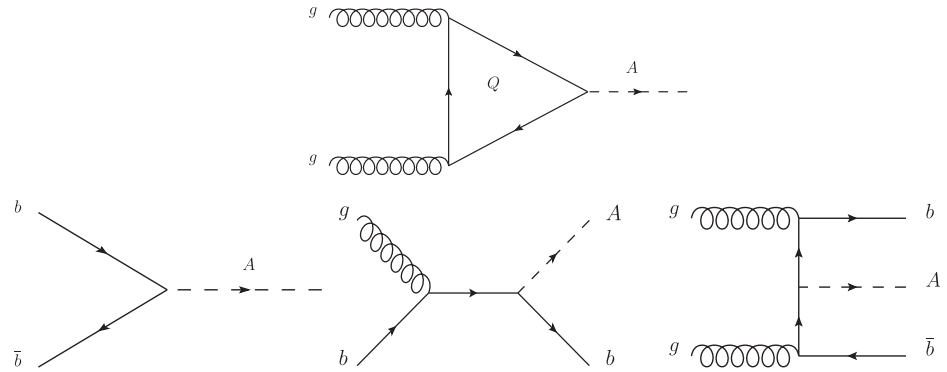

FIG. 1. The Feynman diagrams for the production channels of the *CP*-odd Higgs boson A.

top-quark loop with the large-t_β inputs due to the different t_β dependence in Yukawa couplings, as shown in Table I. Since we have $\xi_A^u = 1/t_\beta$ in both the 2HDM-I and 2HDM-II cases, the top-quark loop in the gluon fusion process will be suppressed for the larger t_β inputs. The bottom-quark associated processes are controlled by the Yukawa coupling of ξ_A^d, which reads $-1/t_\beta$ in 2HDM-I and t_β in 2HDM-II. Therefore, the contributions from these processes become sizable in the 2HDM-II with the large-t_β input. In practice, we evaluate the production cross sections for these processes by SusHi [51]. The inclusive production cross sections of $pp \to AX$ are shown in Fig. 2 for the LHC runs at 14 TeV, where the *CP*-odd Higgs boson is considered in the mass range of $M_A \in (300\,\text{GeV}, 1\,\text{TeV})$. We choose the inputs of $t_\beta = (1, 5, 10)$ for the 2HDM-I case and $t_\beta = (1, 5, 20)$ for the 2HDM-II case, respectively. It is apparent that the inclusive production cross sections of $pp \to AX$ can become sizable with the large-t_β inputs for the 2HDM-II case, where the bottom-quark associated processes become significant. For example, unlike in the 2HDM-I case where the inclusive production cross section of the Higgs boson A decreases with increasing t_β, the production cross section increases in the 2HDM-II case when the t_β value is increased from $t_\beta = 5$ to $t_\beta = 20$, as shown in Fig. 2(b).

B. Decay modes and search signals of A

The tree-level decay channels of A in our discussions here include $A \to (\bar{f}f, hZ, HZ)$, with f being the SM fermions. These partial decay widths are expressed as

$$\Gamma[A \to \bar{f}f] = \frac{N_{c,f} m_f^2 M_A}{8\pi v^2} (\xi_A^f)^2 \sqrt{1 - \frac{4m_f^2}{M_A^2}}, \tag{10a}$$

$$\Gamma[A \to hZ] = \frac{g^2 c_{\beta-\alpha}^2}{64\pi M_A c_W^2} \lambda^{1/2}\left(1, \frac{m_Z^2}{M_A^2}, \frac{M_h^2}{M_A^2}\right) \times \left[m_Z^2 - 2(M_A^2 + M_h^2) + \frac{(M_A^2 - M_h^2)^2}{m_Z^2}\right], \tag{10b}$$

$$\Gamma[A \to HZ] = \frac{g^2 s_{\beta-\alpha}^2}{64\pi M_A c_W^2} \lambda^{1/2}\left(1, \frac{m_Z^2}{M_A^2}, \frac{M_H^2}{M_A^2}\right) \times \left[m_Z^2 - 2(M_A^2 + M_H^2) + \frac{(M_A^2 - M_H^2)^2}{m_Z^2}\right], \tag{10c}$$

with $N_{c,f} = 3(1)$ for quarks (leptons). The three-body phase space factor reads

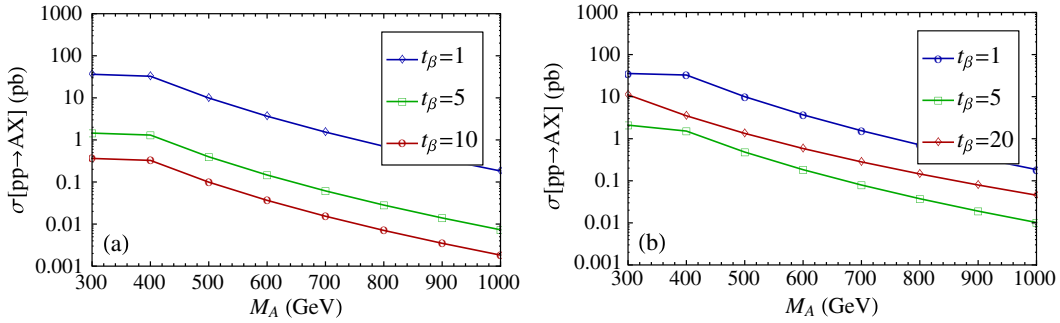

FIG. 2 (color online). The inclusive production cross section $\sigma[pp \to AX]$ for $M_A \in (300\ \text{GeV}, 1\ \text{TeV})$ at the LHC 14 TeV runs. Left: 2HDM-I, with inputs of $t_\beta = 1$ (blue), $t_\beta = 5$ (green), and $t_\beta = 10$ (red). Right: 2HDM-II, with inputs of $t_\beta = 1$ (blue), $t_\beta = 5$ (green), and $t_\beta = 20$ (red).

$$\lambda^{1/2}(1,x^2,y^2) \equiv [(1-x^2-y^2)^2-4x^2y^2]^{1/2}. \quad (11)$$

For the $M_h = M_H = 125$ GeV degenerate scenario, where one cannot discriminate between $A \to hZ$ and $A \to HZ$, one should add up these two decay channels $\Gamma[A \to hZ] + \Gamma[A \to HZ]$, which is collectively denoted as $\Gamma[A \to hZ]$ again in this special case. Thus, the partial width of $\Gamma[A \to hZ]$ in the degenerate scenario becomes independent of the alignment parameter $c_{\beta-\alpha}$

$$\begin{aligned}\Gamma[A \to hZ]_{\rm deg} &= \Gamma[A \to hZ] + \Gamma[A \to HZ] \\ &= \frac{g^2}{64\pi M_A c_W^2}\lambda^{1/2}\left(1,\frac{m_Z^2}{M_A^2},\frac{M_h^2}{M_A^2}\right) \\ &\quad \times \left[m_Z^2 - 2(M_A^2+M_h^2) + \frac{(M_A^2-M_h^2)^2}{m_Z^2}\right]. \end{aligned} \quad (12)$$

The loop-induced partial decay width of $\Gamma[A \to gg]$ was given in Eq. (9b), while other decay widths of $\Gamma[A \to \gamma\gamma]$ and $\Gamma[A \to Z\gamma]$ are typically negligible.

Among all fermionic decay modes, the $A \to \bar{t}t$ is generally the most dominant one except for the large-t_β regions in the 2HDM-II case. It is interesting to compare the partial decay widths of $\Gamma[A \to \bar{t}t]$ and $\Gamma[A \to hZ]$ in the $M_A \gg (m_Z, M_h)$ limit

$$\frac{\Gamma[A \to \bar{t}t]}{\Gamma[A \to hZ]} \approx \frac{8N_{c,f}m_t^2 c_W^2 m_Z^2}{g^2 v^2 M_A^2 t_\beta^2 c_{\beta-\alpha}^2} = 6\left(\frac{m_t}{M_A}\right)^2 \frac{1}{t_\beta^2 c_{\beta-\alpha}^2}. \quad (13)$$

With the large *CP*-odd Higgs boson mass of $M_A \gtrsim 2m_t$, it is quite possible to have $\Gamma[A \to \bar{t}t] \ll \Gamma[A \to hZ]$ with the 2HDM parameters being $c_{\beta-\alpha}^2 t_\beta^2 \gtrsim \mathcal{O}(1)$. Further considering the degenerate scenario of $M_h = M_H = 125$ GeV, the alignment parameter does not enter Eq. (12). Correspondingly, the decay mode of $A \to hZ$ would dominate over the $A \to \bar{t}t$ mode with $M_A \gtrsim 2m_t$. In Figs. 3 and 4, we display the decay branching ratios of the *CP*-odd Higgs boson A in the mass range of $M_A \in (300\ \text{GeV}, 1\ \text{TeV})$ for the 2HDM-I and 2HDM-II cases, respectively. In practice, the decay branching ratios of the *CP*-odd Higgs boson demonstrated here are evaluated by 2HDMC-1.6.4 [52]. In Figs. 3 and 4, we demonstrate the branching ratios for both the $M_h = 125$ GeV scenario and the $M_h = M_H = 125$ GeV degenerate scenario. The decay branching ratios of $\text{BR}[A \to hZ]$ are increasing with the larger M_A and t_β inputs. For the $M_h = 125$ GeV scenario, the $\text{BR}[A \to hZ]$ increases from $\mathcal{O}(0.1)$ to almost unity with the increase of t_β from 1 to 10 in the 2HDM-I case. However, in the 2HDM-II case, this decay mode is always subdominant for both small- and large-t_β inputs, given the small alignment parameter taken in Eq. (8). For the $M_h = M_H = 125$ GeV scenario, the $\text{BR}[A \to hZ]$ can be the most dominant one over the mass range we are interested in.

Figure 5 shows the $\sigma[pp \to AX] \times \text{BR}[A \to hZ]$ for various cases at the LHC 14 TeV runs. This is done by combining the inclusive production cross sections of $\sigma[pp \to AX]$ displayed in Fig. 2 and the decay branching ratios of $\text{BR}[A \to hZ]$ displayed in Figs. 3 and 4 for the 2HDM-I and 2HDM-II cases, respectively. In descending

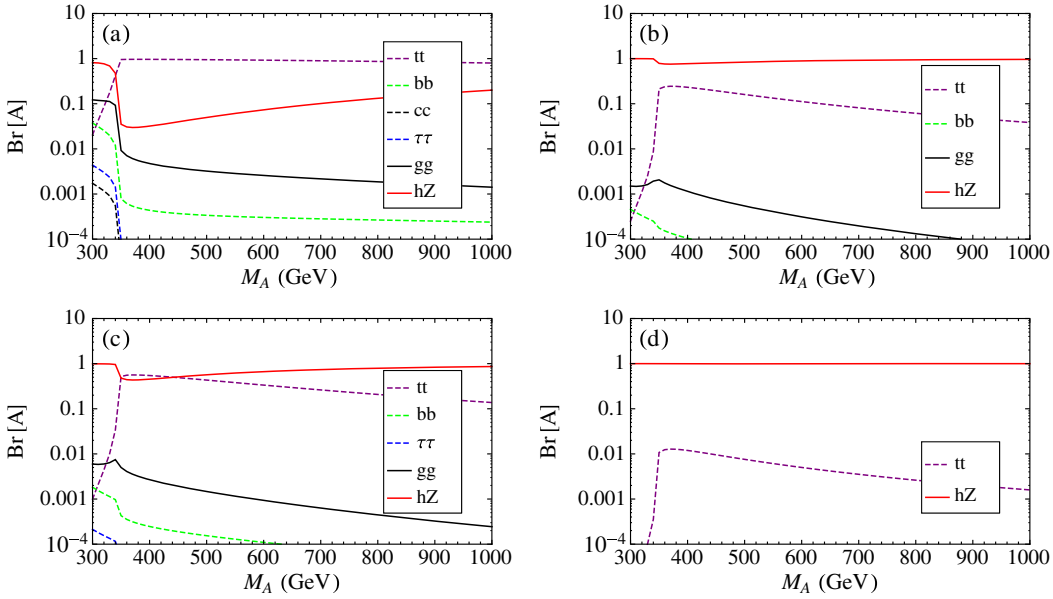

FIG. 3 (color online). The decay branching ratios of the *CP*-odd Higgs boson $\text{BR}[A]$ for the 2HDM-I case. (a) $M_h = 125$ GeV with $t_\beta = 1$. (b) $M_h = 125$ GeV with $t_\beta = 10$. (c) $M_h = M_H = 125$ GeV with $t_\beta = 1$. (d) $M_h = M_H = 125$ GeV with $t_\beta = 10$. The decay channels with branching ratios below 10^{-4} are not shown.

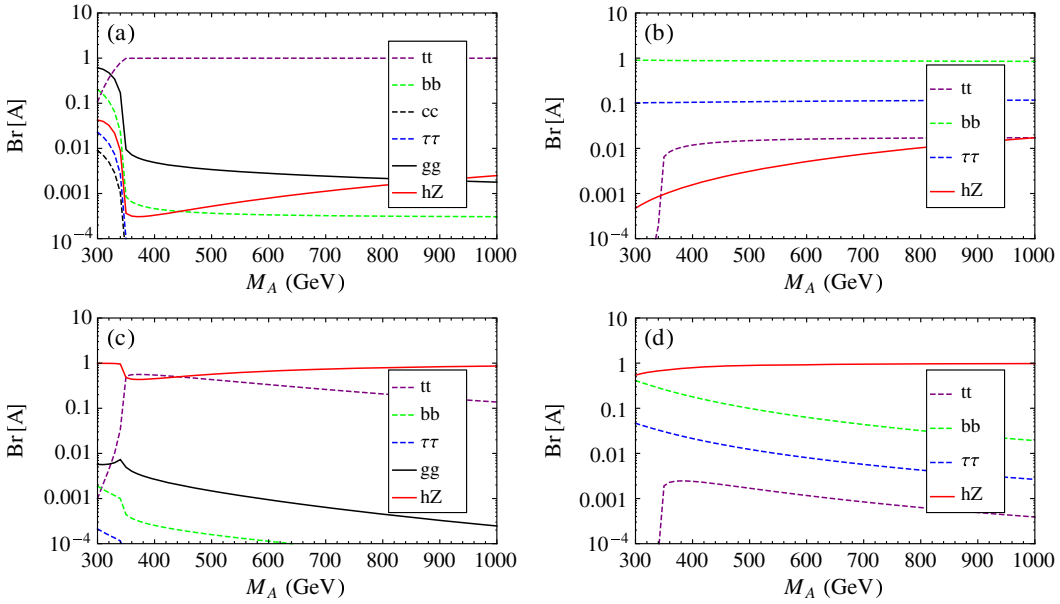

FIG. 4 (color online). The decay branching ratios of the *CP*-odd Higgs boson BR$[A]$ for the 2HDM-II case. (a) $M_h = 125$ GeV with $t_\beta = 1$. (b) $M_h = 125$ GeV with $t_\beta = 20$. (c) $M_h = M_H = 125$ GeV with $t_\beta = 1$. (d) $M_h = M_H = 125$ GeV with $t_\beta = 20$. The decay channels with branching ratios below 10^{-4} are not shown.

order, the curves correspond to input parameters of $t_\beta = 1, 5, 10$ for the 2HDM-I signal predictions. This is largely due to the production cross section dependence on the t_β inputs, as shown in Fig. 2(a). Meanwhile, the corresponding decay branching ratio of BR$[A \to hZ]$ for the 2HDM-I case varies moderately in the range of $\mathcal{O}(0.1) - \mathcal{O}(1)$, as shown in Fig. 3. Therefore, the search for the *CP*-odd Higgs boson via the $A \to hZ$ channel is possible for the 2HDM-I cases at the LHC 14 TeV runs, with the integrated luminosities accumulated up to $\mathcal{O}(10^3)$ fb^{-1}. In comparison, the signal predictions of $\sigma[pp \to AX] \times \mathrm{BR}[A \to hZ]$ for the 2HDM-II with the $M_h = 125$ GeV case are highly suppressed to $\mathcal{O}(10^{-2}) - \mathcal{O}(10^{-3})$ pb with $M_A \gtrsim 2m_t$. This is obvious as seen from the more dominant decay modes of $A \to \bar{t}t$ for the small $t_\beta = 1$ input and $A \to (\bar{b}b, \tau^+\tau^-)$ for the large $t_\beta = 20$

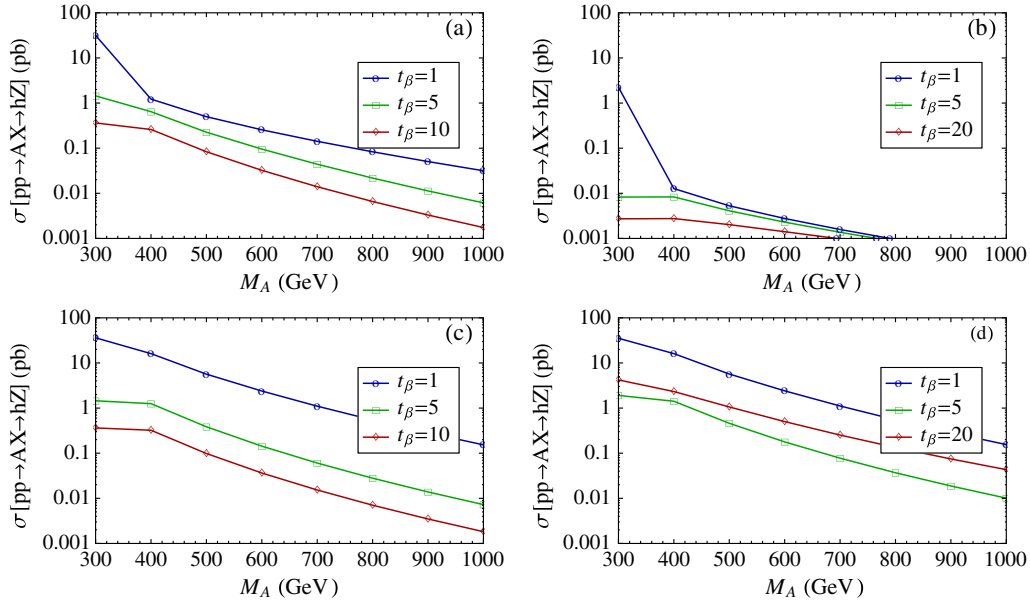

FIG. 5 (color online). The $\sigma[pp \to AX] \times \mathrm{BR}[A \to hZ]$ for $M_A \in (300\ \mathrm{GeV}, 1\ \mathrm{TeV})$ at the LHC 14 TeV runs. (a) $M_h = 125$ GeV for 2HDM-I. (b) $M_h = 125$ GeV for 2HDM-II. (c) $M_h = M_H = 125$ GeV for 2HDM-I. (d) $M_h = M_H = 125$ GeV for 2HDM-II.

input, respectively. Thus, the search channel of $A \to hZ$ at the LHC 14 TeV run is of minor interest for the 2HDM-II with the $M_h = 125$ GeV case, as will be shown in the following section. For the 2HDM-II with the $M_h = M_H = 125$ GeV cases, the decay mode of $A \to hZ$ is always $\sim\mathcal{O}(1)$ with various (M_A, t_β) parameters. Therefore, the signal predictions of $\sigma[pp \to AX] \times \mathrm{BR}[A \to hZ]$ roughly follow the same manner as the CP-odd Higgs productions, as given in Fig. 2(b) earlier.

For the $M_h = 125$ GeV scenario, in the 2HDM-I case, this decay mode of $A \to hZ$ can be the possible search channel for the CP-odd Higgs boson as heavy as $\sim$1 TeV with t_β being not too large; in the 2HDM-II case, however, the search potential to the $A \to hZ$ mode is much smaller because the cross section in this case is typically small. For the $M_h = M_H = 125$ GeV degenerate scenario, the search potential to the $A \to hZ$ mode is significantly improved for both the 2HDM-I and the 2HDM-II cases. By simple counting of the $\sigma[pp \to AX] \times \mathrm{BR}[A \to hZ]$, one can envision this decay mode to be promising for M_A as large as $\mathcal{O}(1)$ TeV at the LHC 14 TeV runs with the integrated luminosity up to $\sim\mathcal{O}(100) - \mathcal{O}(10^3)$ fb^{-1}. In our analysis below, we shall use the $h/H \to \bar{b}b$ final states in order to tag the fat Higgs jet. For this reason, the cross sections for the signal processes read

$$M_h = 125\ \mathrm{GeV}: \sigma[pp \to AZ] \times \mathrm{BR}[A \to hZ] \times \mathrm{BR}[h \to \bar{b}b], \tag{14a}$$

$$\begin{aligned} M_h = M_H = 125\ \mathrm{GeV}: \ & \sigma[pp \to AZ] \\ & \times (\mathrm{BR}[A \to hZ] \times \mathrm{BR}[h \to \bar{b}b] \\ & + \mathrm{BR}[A \to HZ] \times \mathrm{BR}[H \to \bar{b}b]), \end{aligned} \tag{14b}$$

respectively. In the $M_h = 125$ GeV scenario, the current global fit to the 2HDM parameter regions of (α, β) points to a SM-like Higgs boson h. Hence, it is reasonable to take $\mathrm{BR}[h \to \bar{b}b] \approx \mathrm{BR}[h_{\mathrm{SM}} \to \bar{b}b] = 0.58$ for our estimation of the signal cross sections below. In the $M_h = M_H = 125$ GeV scenario, however, a global fit to the 125 GeV Higgs boson is lacking. One can further write the branching ratios in Eq. (14b) as

$$\begin{aligned} & \mathrm{BR}[A \to hZ] \times \mathrm{BR}[h \to \bar{b}b] + \mathrm{BR}[A \to HZ] \times \mathrm{BR}[H \to \bar{b}b] \\ & \quad = \mathrm{BR}[A \to hZ]_{\mathrm{deg}} \times (c^2_{\beta-\alpha} \mathrm{BR}[h \to \bar{b}b] \\ & \qquad + s^2_{\beta-\alpha} \mathrm{BR}[H \to \bar{b}b]), \end{aligned} \tag{15}$$

where we used Eqs. (10b), (10c), and (12) in the last line. Instead of constraining the 2HDM parameters for the $M_h = M_H = 125$ GeV scenario, here we assume that the branching ratios in the parentheses reproduce the SM value, i.e., $c^2_{\beta-\alpha}\mathrm{BR}[h \to \bar{b}b] + s^2_{\beta-\alpha}\mathrm{BR}[H \to \bar{b}b] \approx \mathrm{BR}[h_{\mathrm{SM}} \to \bar{b}b] = 0.58$. This approximation is reasonable if we assume the future LHC searches for the $\bar{b}b$ final states via the $pp \to Vh(\to \bar{b}b)$ process are close to the SM Higgs predictions.

IV. LHC SEARCHES FOR THE EXOTIC $A \to hZ$ CHANNEL

In this section, we proceed to analyze the LHC searches for the CP-odd Higgs boson A via the decay mode of $A \to hZ$.

A. SM backgrounds and signal benchmark

The final states to be searched for are the same as the ones in the SM Higgs boson searches via the hZ-associated production channel. Therefore, the dominant irreducible SM backgrounds relevant to our analysis are [53] $\bar{b}b\ell^+\ell^-$, $\bar{t}t$, $ZZ \to \bar{b}b\ell^+\ell^-$, and the $h_{\mathrm{SM}}Z \to \bar{b}b\ell^+\ell^-$. The cross sections for these processes [54–57] at the LHC 14 TeV run read

$$\begin{aligned} \sigma(pp \to \bar{t}t) &\approx 855\ \mathrm{pb}, \\ \sigma(pp \to \bar{b}b\ell^+\ell^-) &\approx 82\ \mathrm{pb}, \\ \sigma(pp \to ZZ \to \bar{b}b\ell^+\ell^-) &\approx 180\ \mathrm{fb}, \\ \sigma(pp \to h_{\mathrm{SM}}Z \to \bar{b}b\ell^+\ell^-) &\approx 34\ \mathrm{fb}. \end{aligned} \tag{16}$$

In practice, we note the major SM background processes of $\bar{t}t$ and $\bar{b}b\ell^+\ell^-$ receive uncertainties of $\sim$9% and $\sim$14%, respectively. In our analysis below, we take the b-tagging efficiency of 70% [58], and the mistagging rates are taken as

$$\epsilon_{c\to b} \approx 0.2, \qquad \epsilon_{j\to b} \approx 0.01, \tag{17}$$

with j representing the light jets that neither originate from a b quark or a c quark [59].

In order to generate events for the signal processes, we obtain a Universal FeynRules Output [60] simplified model with A being the only particle beyond the standard model. The relevant coupling terms are implemented, namely, the dimension-five Agg coupling, the derivative coupling of AhZ, and the $A(h)\bar{b}b$ Yukawa couplings. We generate events at the parton level by Madgraph 5 [61], which are passed to Pythia [62] for the parton showering and hadronization. In order to employ the fat Higgs jet tagging method [38], the B-hadron decays are turned off. All events are further passed to Delphes-3.1.2 [63] for the fast detector simulation, where we apply the default ATLAS detector card. The Delphes output will be used for the jet substructure analysis by Fastjet [64].

B. Jet substructure methods

Here we describe the jet substructure analysis and the application to the signals we are interested in. The tracks, neutral hadrons, and photons that enter the jet

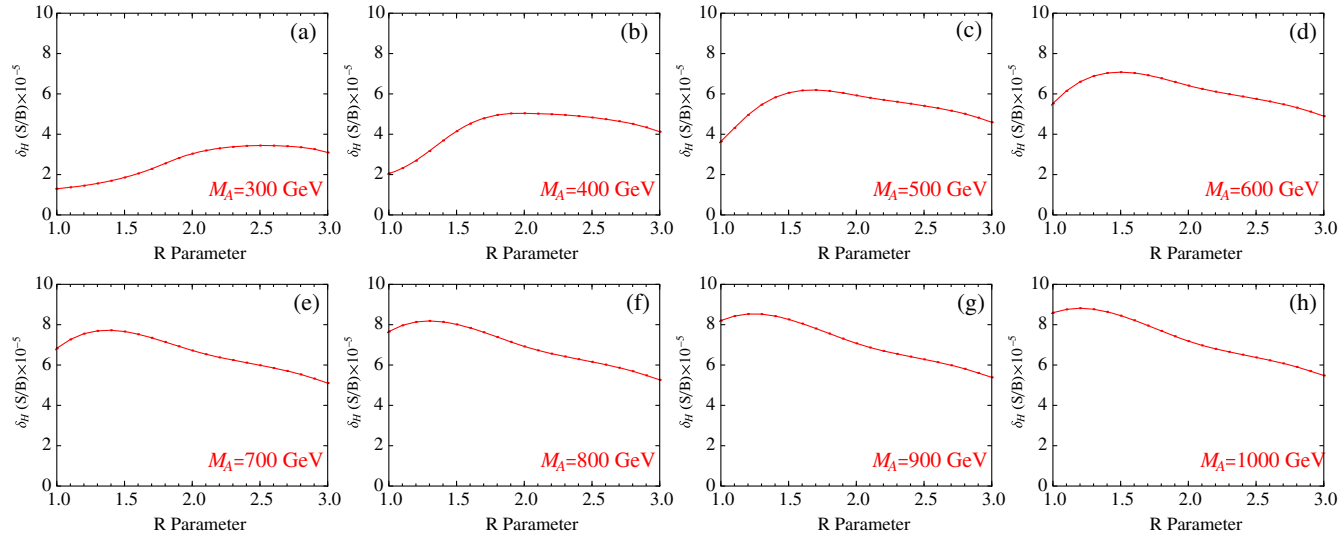

FIG. 6 (color online). The fat Higgs jet tagging rates $\delta_H(S/B)$ with the varying jet cone sizes R in the CA jet algorithm. For comparison, we take a common cross section of $\sigma[pp \to AX \to hZ] = 100$ fb for all signal processes. Plots (a)–(h) correspond to the fat Higgs jet tagging rates for the $M_A = (300, 400, 500, 600, 700, 800, 900, 1000)$ GeV cases.

reconstruction should satisfy $p_T > 0.1$ GeV and $|\eta| < 5.0$. The leptons from the events should be isolated, so that they will not be used to cluster the fat jets. The fat jets are reconstructed by using the CA jet algorithm with particular jet cone size R to be specified below and requiring $p_T > 30$ GeV. Afterwards, we adopt the procedures described in the mass-drop tagger [38] for the purpose of identifying a boosted Higgs boson:

(i) Split the fat jet j into two subjets $j_{1,2}$ with masses $m_{1,2}$, and $m_1 > m_2$.

(ii) Require a significant mass drop of $m_1 < \mu m_j$ with $\mu = 0.667$, and also a sufficiently symmetric splitting of $\min(p_{T,1}^2, p_{T,2}^2)\Delta R_{12}^2/m_j^2 > y_{\rm cut}$ (ΔR_{12}^2 is the angular distance between j_1 and j_2 on the $\eta - \phi$ plane) with $y_{\rm cut} = 0.09$.

(iii) If the above criteria are not satisfied, define $j \equiv j_1$ and go back to the first step for decomposition.

These steps are followed by the filtering stage using the reclustering radius of $R_{\rm filt} = \min(0.35, R_{12}/2)$ and selecting the three hardest subjects to suppress the pileup effects.

Generally, the jet cone size R taken in the CA algorithm tends to be large in order to capture all collimated decay products in a fat jet. Since our final states involve a SM-like Higgs boson h from the $A \to hZ$ decay, the corresponding boost factors are enhanced for the larger M_A case. To determine the most optimal jet cone size R in the CA jet algorithm choice for each M_A input, we vary it in the range of $1.0 \le R \le 3.0$ and look for the maximal fat Higgs jet tagging rates $\delta_H(S/B)$

$$\delta_H(S/B) \equiv \frac{\text{number of Higgs jets tagged in the signal}}{\sum_{\rm background} \text{number of Higgs jets tagged in SM background}} \tag{18}$$

between the signals and SM backgrounds. In Fig. 6, we demonstrated the fat Higgs jet tagging rate δ_H for different M_A samples with the varying $1.0 \le R \le 3.0$. Accordingly, the most optimal jet cone size R to be chosen for each M_A input is tabulated in Table II. As seen from the table, a smaller cone size R is generally favored for the heavier CP-odd Higgs boson.

C. Event selection

The cut flow we impose to the events is the following:

(i) Cut 1: We select events with the opposite-sign-same-flavor (OSSF) dileptons $(\ell^+\ell^-)$ in order to reconstruct the final-state Z boson. The OSSF dileptons are required to satisfy the following selection cuts

TABLE II. The choices of the jet cone sizes R in the CA jet algorithm for different M_A inputs.

M_A	300 GeV	400 GeV	500 GeV	600 GeV
CA algorithm R	2.5	2.0	1.7	1.5
M_A	700 GeV	800 GeV	900 GeV	1000 GeV
CA algorithm R	1.4	1.3	1.2	1.2

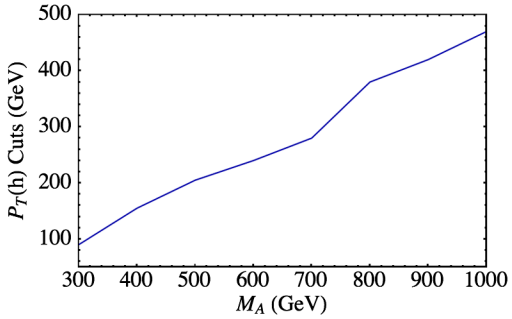

FIG. 7 (color online). The most optimal cuts to the p_T of the tagged SM-like Higgs boson for different M_A inputs.

$$|\eta_\ell| < 2.5, \quad p_T(\ell_1) \geq 20\,\text{GeV}, \quad p_T(\ell_2) \geq 10\,\text{GeV}, \tag{19}$$

where $\ell_{1,2}$ represent two leading leptons ordered by their transverse momenta.

(ii) Cut 2: The invariant mass of the selected OSSF dileptons should be around the mass window of the Z boson $|m_{\ell\ell} - m_Z| \leq 15$ GeV.

(iii) Cut 3: At least one filtered fat jet is required, which should also contain two leading subjets that pass the b tagging and satisfy $p_T > 20$ GeV and $|\eta| < 2.5$.

(iv) Cut 4: Such a filtered fat jet will be then identified as the SM-like Higgs jet. We impose the cuts to the filtered Higgs jets in the mass window of $M_h(\text{tagged}) \in (100\,\text{GeV}, 150\,\text{GeV})$.

(v) Cut 5: We also impose the cuts on the $p_{T,h}(\text{tagged})$. The SM-like Higgs bosons decaying from the heavier *CP*-odd Higgs boson A would generally be more boosted. In practice, we vary the $p_{T,h}(\text{tagged})_{\text{cut}} \in (50\,\text{GeV}, 500\,\text{GeV})$ and look for the most optimal cuts on $p_{T,h}(\text{tagged})$ by counting the corresponding cut efficiencies of S/B. The $p_{T,h}(\text{tagged})$ cuts to be adopted below are displayed in Fig. 7.

(vi) Cut 6: Combining the filtered Higgs jets and the tagged OSSF dileptons, the invariant mass of the tagged Higgs boson and the OSSF leptons should reconstruct the mass window of the *CP*-odd Higgs boson A: $|M_{h,\ell^+\ell^-} - M_A| \leq 100$ GeV.

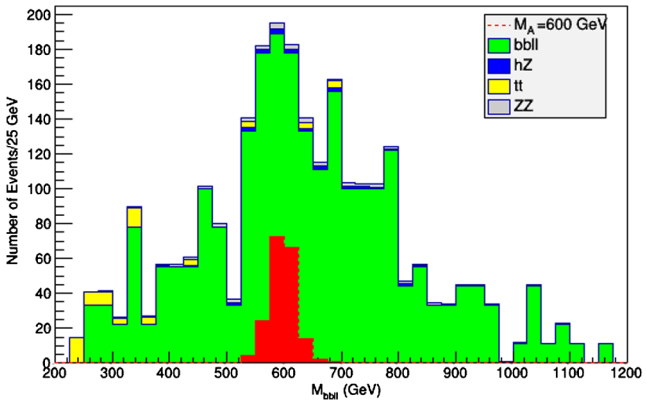

FIG. 8 (color online). The $M_{h,ll}$ distributions of the $pp \to AX \to hZ$ signal process (for the $M_A = 600$ GeV case) and all SM background processes after the kinematic cuts. A nominal cross section of $\sigma[pp \to AX] \times \text{BR}[A \to hZ] = 500$ fb is assumed for the signal. The plot is for the LHC 14 TeV run with integrated luminosity of $\int \mathcal{L}dt = 100$ fb^{-1}.

D. Implications to the LHC searches for A in the general 2HDM

Here we present the results after the jet substructure analysis and imposing the kinematic cuts stated previously. As a specific example of the analysis stated above, we list the cut efficiencies for the benchmark model for the $M_A = 600$ GeV case in Table III. The distributions of the $M_{h,\ell\ell}$ after Cut 1 through Cut 5 for both signal process and the relevant SM background processes are displayed in Fig. 8. A nominal production cross section of $\sigma[pp \to AX] \times \text{BR}[A \to hZ] = 500$ fb for the signal process is chosen for the evaluation. Among all relevant SM background processes, the $\bar{b}b\ell^+\ell^-$ turns out to contribute most after imposing the cuts mentioned above.

In Figs. 9 and 10, we display the number of events predicted by the signal process of $pp \to AX \to hZ$ after the cut flows imposed to the 2HDM-I and 2HDM-II models, respectively. For each M_A sample, the same kinematic cuts

TABLE III. The event cut efficiency for the $M_A = 600$ GeV case at the LHC 14 TeV running of the signal and background processes. We assume the nominal cross section for the signal process to be $\sigma[pp \to AX] \times \text{BR}[A \to hZ] = 500$ fb. The $S/\sqrt{B}$ is evaluated for the $\int \mathcal{L}dt = 100$ fb^{-1} case. The uncertainties of the SM background processes are taken into account.

Cuts	$A \to hZ$	$\bar{t}t$	$\bar{b}b\ell^+\ell^-$	$ZZ \to \bar{b}b\ell^+\ell^-$	$hZ \to \bar{b}b\ell^+\ell^-$	S/B	$S/\sqrt{B}$
Total cross section (fb)	500	8.6×10^5	8.2×10^4	180	34	⋯	
Cut 1	10.76	1.0×10^4	4.3×10^4	98.94	0.81	1.3×10^{-4}	0.47
Cut 2	10.29	2061	3.9×10^4	93.49	0.78	1.6×10^{-4}	0.51
Cut 3	2.41	120.63	1759	4.92	0.05	8.2×10^{-4}	0.56
Cut 4	1.38	13.12	100.54	1.12	0.03	7.7×10^{-3}	1.29
Cut 5	0.91	0.38	12.14	0.19	0.01	0.04	2.55
Cut 6	0.91	0.06	5.40	0.08	⋯	0.10	3.87

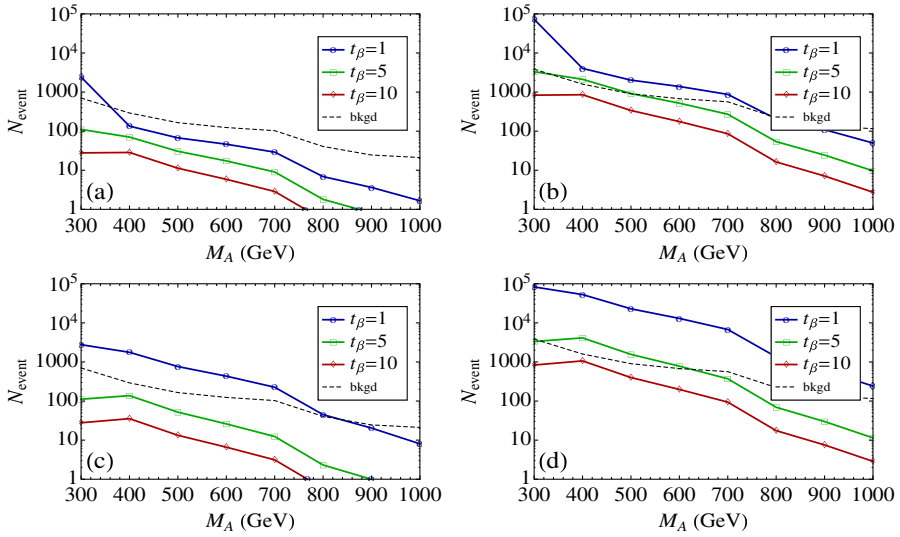

FIG. 9 (color online). The number of events for the $pp \to AX \to hZ$ signal in the 2HDM-I and the corresponding SM background processes after the jet substructure analysis. (a) $M_h = 125$ GeV for $\int \mathcal{L}dt = 100$ fb^{-1}. (b) $M_h = 125$ GeV for $\int \mathcal{L}dt = 3000$ fb^{-1}. (c) $M_h = M_H = 125$ GeV for $\int \mathcal{L}dt = 100$ fb^{-1}. (d) $M_h = M_H = 125$ GeV for $\int \mathcal{L}dt = 3000$ fb^{-1}. We show samples with $t_\beta = 1$ (blue), $t_\beta = 5$ (green), and $t_\beta = 10$ (red) for each plot. The discovery limit (dashed black curve) of $\max\{5\sqrt{B}, 10\}$ is demonstrated for each plot.

were also imposed to the SM background processes. The samples with different t_β inputs are shown for both the $M_h = 125$ GeV scenario and the $M_h = M_H = 125$ GeV degenerate scenario. We demonstrate the predictions at the LHC 14 TeV runs with integrated luminosities of 100 fb^{-1} and high luminosity (HL) runs up to 3000 fb^{-1}. Altogether, the 5σ discovery limits set by $\max\{5\sqrt{B}, 10\}$ with B representing the number of events from the SM background contributions are also shown. For the 2HDM-I cases, the $M_h = 125$ GeV scenario consistent with the current global fit to the 2HDM parameter is likely to be probed with M_A up to 1 TeV with the integrated luminosity ~3000 fb^{-1}. For

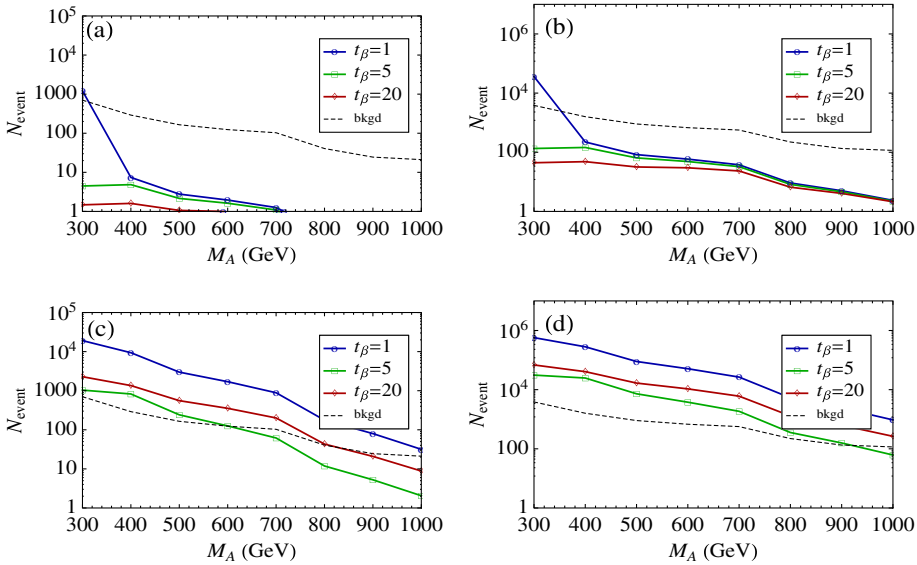

FIG. 10 (color online). The number of events for the $pp \to AX \to hZ$ signal in the 2HDM-II and the corresponding SM background processes after the jet substructure analysis. (a) $M_h = 125$ GeV for $\int \mathcal{L}dt = 100$ fb^{-1}. (b) $M_h = 125$ GeV for $\int \mathcal{L}dt = 3000$ fb^{-1}. (c) $M_h = M_H = 125$ GeV for $\int \mathcal{L}dt = 100$ fb^{-1}. (d) $M_h = M_H = 125$ GeV for $\int \mathcal{L}dt = 3000$ fb^{-1}. We show samples with $t_\beta = 1$ (blue), $t_\beta = 5$ (green), and $t_\beta = 20$ (red) for each plot. The discovery limit (dashed black curve) of $\max\{5\sqrt{B}, 10\}$ is demonstrated for each plot.

the special $M_h = M_H = 125$ GeV degenerate scenario, the discovery limit to the M_A can reach ∼1 TeV at the LHC 14 TeV runs with $\int \mathcal{L}dt \sim 100$ fb^{-1}. The increasing integrated luminosities would further enhance the discovery limits for models with larger t_β inputs. Situations for the 2HDM-II cases are different. The $M_h = 125$ GeV scenario is not promising even at the HL LHC runs with integrated luminosities up to ∼3000 fb^{-1}. Only the *CP*-odd Higgs boson with mass of $M_A \lesssim 2m_t$ is likely to be searched, together within the low-t_β regions. On the other hand, the $M_h = M_H = 125$ GeV degenerate scenario is promising to search for, as indicated from the previous results shown in Fig. 5(d). As the production cross sections are dominated by the gluon fusion at the low-t_β regions, while the bottom-quark associated processes can be enhanced at the high-t_β regions, Figs. 10(c) and 10(d) suggest this channel is promising for the 2HDM-II under the degenerate scenario.

The signal reaches on the (M_A, t_β) plane are further displayed in Figs. 11 and 12 for the 2HDM-I and 2HDM-II cases, respectively. For the samples we study, both the scenarios of $M_h = 125$ GeV and $M_h = M_H = 125$ GeV are shown. There are significant improvements of the signal reaches when increasing the integrated luminosity from 100 fb^{-1} up to the HL LHC runs up to 3000 fb^{-1}. For the 2HDM-I case, the $\sigma[pp \to AX] \times \mathrm{BR}[A \to hZ]$ decreases with the larger t_β inputs, as is consistent with what is presented in Figs. 5(a) and 5(b). Correspondingly, this search channel of $A \to hZ$ is generally promising for the low-t_β regions. However, for the 2HDM-II case, the large-t_β regions are also possible for the search channel of $A \to hZ$. This is true for the special $M_h = M_H = 125$ GeV degenerate scenario. Therefore, one would envision the results presented here are generally complementary to the conventional experimental searches via the $A \to \bar{b}b$ and $A \to \tau^+\tau^-$ final states.

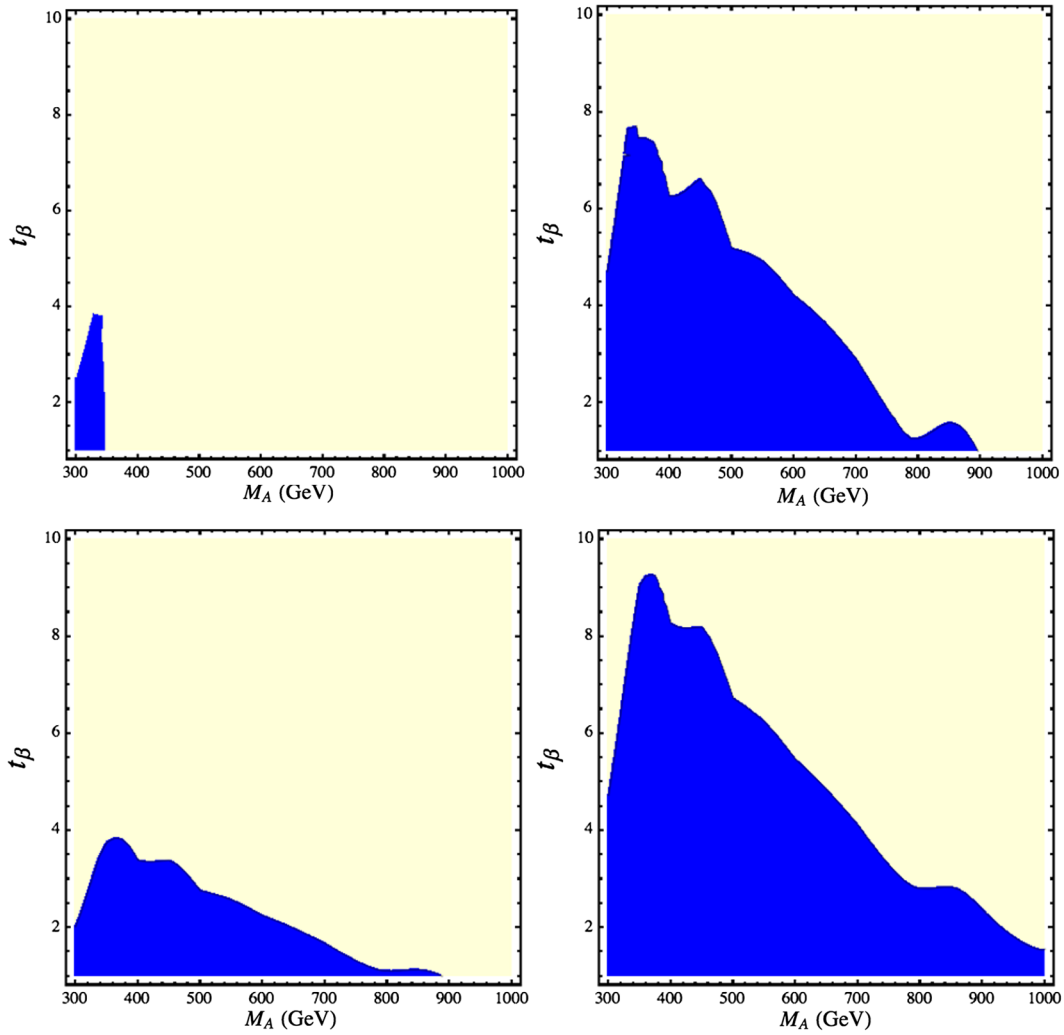

FIG. 11 (color online). The signal reaches for the $A \to hZ$ on the (M_A, t_β) plane for the 2HDM-I case. Upper left: $M_h = 125$ GeV for $\int \mathcal{L}dt = 100$ fb^{-1}. Upper right: $M_h = 125$ GeV for $\int \mathcal{L}dt = 3000$ fb^{-1}. Lower left: $M_h = M_H = 125$ GeV for $\int \mathcal{L}dt = 100$ fb^{-1}. Lower right: $M_h = M_H = 125$ GeV for $\int \mathcal{L}dt = 3000$ fb^{-1}. Parameter regions of (M_A, t_β) in blue are within the reach for each case.

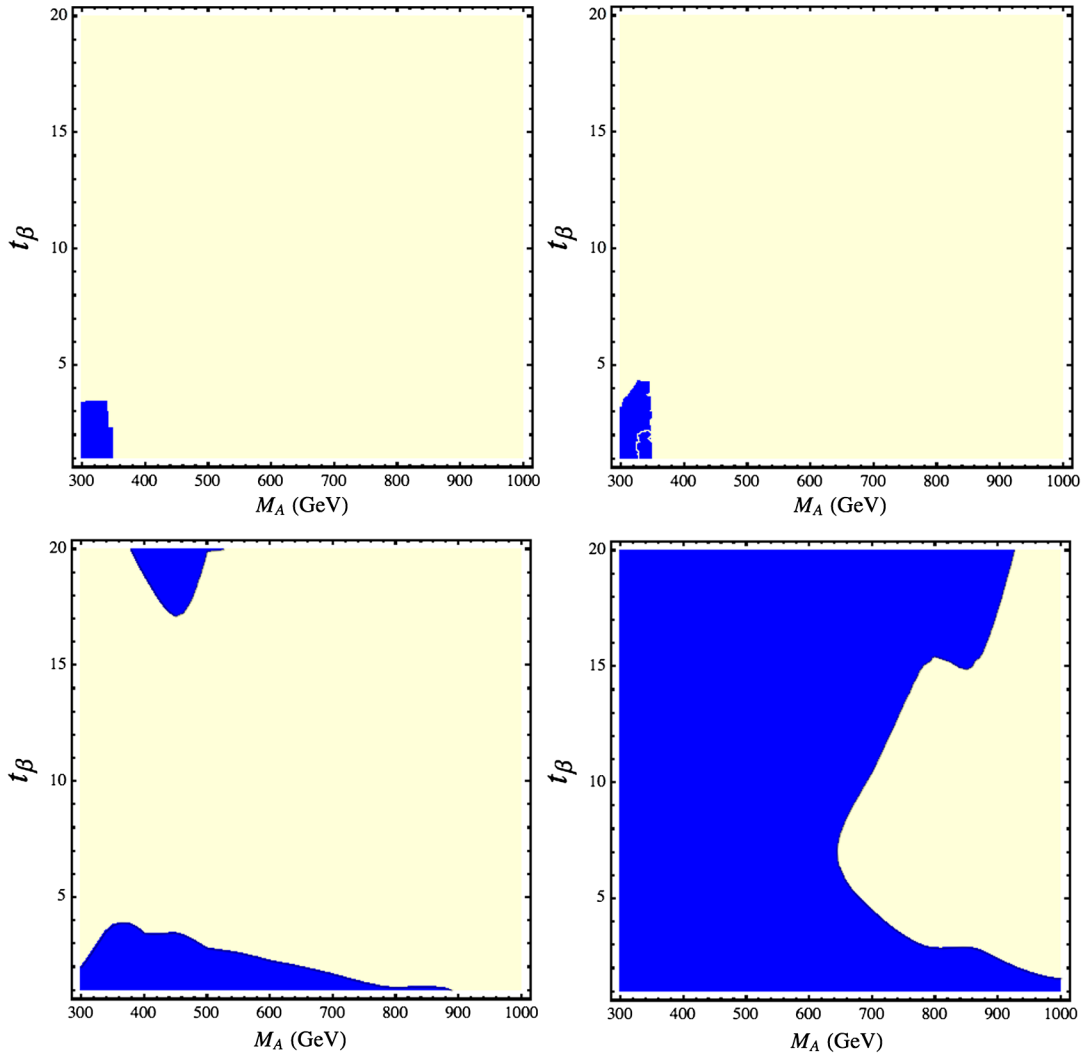

FIG. 12 (color online). The signal reaches for the $A \to hZ$ on the (M_A, t_β) plane for the 2HDM-II case. Upper left: $M_h = 125$ GeV for $\int \mathcal{L}dt = 100$ fb^{-1}. Upper right: $M_h = 125$ GeV for $\int \mathcal{L}dt = 3000$ fb^{-1}. Lower left: $M_h = M_H = 125$ GeV for $\int \mathcal{L}dt = 100$ fb^{-1}. Lower right: $M_h = M_H = 125$ GeV for $\int \mathcal{L}dt = 3000$ fb^{-1}. Parameter regions of (M_A, t_β) in blue are within the reach for each case.

V. CONCLUSION

In this work, we suggested that searches for the hZ final states of a heavy CP-odd Higgs boson A in the general 2HDM can be considered as a potentially promising channel for the upcoming LHC runs at 14 TeV. Such a decay channel is due to the derivative coupling term AhZ arising from the 2HDM kinematic terms. Within the framework of the general 2HDM, we consider this decay channel for two scenarios, i.e., the $M_h = 125$ GeV case and the $M_h = M_H = 125$ GeV degenerate Higgs case. For the first scenario, the global fit to the 125 GeV Higgs boson in the context of the 2HDM is applied. By comparing the decay branching ratios of BR$[A \to hZ]$ with other decay modes, together with the evaluation of the inclusive production cross sections for the CP-odd Higgs boson, it is shown that this channel can become the leading one for consideration. Furthermore, the technique of tagging the boosted Higgs jets from the $A \to hZ$ decay chain is very efficient for suppressing the SM background contributions. We optimized the jet cone size R in the CA jet algorithm so that the Higgs tagging rates in each signal process were maximized compared to the SM background contributions. The cut flows to capture the kinematical features for the signal processes were applied thereafter. In particular, we optimize the p_T cut to the tagged Higgs jets. Based on the analysis, the signal reaches for the $A \to hZ$ channel were obtained. The mass reach can be generally up to $\sim\mathcal{O}(1)$ TeV for the 2HDM-I with low-t_β inputs at the HL LHC runs. The search mode is mostly interesting in the special $M_h = M_H = 125$ GeV degenerate scenario for the 2HDM-II case, both for the low-t_β and large-t_β regions. However, for the $M_h = 125$ GeV scenario in the 2HDM-II, there exist stringent constraints on the

alignment parameter $c_{\beta-\alpha}$ from the current global fit to the 125 GeV Higgs boson signal strengths. Therefore, this decay mode of $A \to hZ$ is highly suppressed in this case, unless the further results from the LHC measurements of the 125 GeV Higgs boson would modify the constraints significantly.

In a more generic context with a 2HDM setup as the low-energy description in the scalar sector, this decay mode of $A \to hZ$ exists. Studies to this decay mode for the *CP*-odd Higgs boson searches are of general interest in this sense for the future experiments. In particular, the analysis of the boosted Higgs jet from this channel can be similarly applied. As we have shown the sensitivity regions on the (M_A, t_β) plane via this channel, the searches for the $A \to hZ$ mode can become complementary to the conventional search modes of $A \to \bar{b}b$ and $A \to \tau^+\tau^+$.

ACKNOWLEDGMENTS

We would like to thank Yun Jiang for useful discussions. This work is partially supported by the National Science Foundation of China (under Grants No. 11275009 and No. 11335007), the Tsinghua University Talent Fund (under Grant No. 543481001), and the Australian Research Council (under Grant No. CE110001004). N. C. would like to thank the Center of High Energy Physics (CHEP) of Peking University for their hospitality when part of this work was prepared.

[1] P. W. Higgs, Phys. Lett. **12**, 132 (1964).
[2] P. W. Higgs, Phys. Rev. Lett. **13**, 508 (1964).
[3] F. Englert and R. Brout, Phys. Rev. Lett. **13**, 321 (1964).
[4] M. E. Peskin, arXiv:1207.2516.
[5] A. Djouadi, R. M. Godbole, B. Mellado, and K. Mohan, Phys. Lett. B **723**, 307 (2013).
[6] D. Curtin, R. Essig, S. Gori, P. Jaiswal, A. Katz, T. Liu, Z. Liu, D. McKeen *et al.*, Phys. Rev. D **90**, 075004 (2014).
[7] S. Dimopoulos and H. Georgi, Nucl. Phys. **B193**, 150 (1981).
[8] Z. Chacko, Y. Nomura, M. Papucci, and G. Perez, J. High Energy Phys. 01 (2006) 126.
[9] J. Mrazek, A. Pomarol, R. Rattazzi, M. Redi, J. Serra, and A. Wulzer, Nucl. Phys. **B853**, 1 (2011).
[10] G. C. Branco, P. M. Ferreira, L. Lavoura, M. N. Rebelo, M. Sher, and J. P. Silva, Phys. Rep. **516**, 1 (2012).
[11] N. Craig and S. Thomas, J. High Energy Phys. 11 (2012) 083.
[12] N. Craig, J. A. Evans, R. Gray, C. Kilic, M. Park, S. Somalwar, and S. Thomas, J. High Energy Phys. 02 (2013) 033.
[13] B. Coleppa, F. Kling, and S. Su, J. High Energy Phys. 01 (2014) 161.
[14] N. Craig, J. Galloway, and S. Thomas, arXiv:1305.2424.
[15] B. Coleppa, F. Kling, and S. Su, arXiv:1308.6201.
[16] M. Carena, I. Low, N. R. Shah, and C. E. M. Wagner, J. High Energy Phys. 04 (2014) 015.
[17] N. Chen, C. Du, Y. Fang, and L. C. Lü, Phys. Rev. D **89**, 115006 (2014).
[18] J. Baglio, O. Eberhardt, U. Nierste, and M. Wiebusch, Phys. Rev. D **90**, 015008 (2014).
[19] B. Coleppa, F. Kling, and S. Su, J. High Energy Phys. 09 (2014) 161.
[20] B. Dumont, J. F. Gunion, Y. Jiang, and S. Kraml, Phys. Rev. D **90**, 035021 (2014).
[21] G. C. Dorsch, S. Huber, K. Mimasu, and J. M. No, Phys. Rev. Lett. **113**, 211802 (2014).
[22] B. Hespel, D. Lopez-Val, and E. Vryonidou, J. High Energy Phys. 09 (2014) 124.
[23] V. Barger, L. L. Everett, C. B. Jackson, A. D. Peterson, and G. Shaughnessy, Phys. Rev. D **90**, 095006 (2014).
[24] D. Fontes, J. C. Romo, and J. P. Silva, J. High Energy Phys. 12 (2014) 043.
[25] B. Coleppa, F. Kling, and S. Su, J. High Energy Phys. 12 (2014) 148.
[26] B. Grzadkowski, O. M. Ogreid, and P. Osland, J. High Energy Phys. 11 (2014) 084.
[27] J. F. Gunion, Y. Jiang, and S. Kraml, Phys. Rev. Lett. **110**, 051801 (2013).
[28] T. Aaltonen *et al.* (CDF and D0 Collaborations), Phys. Rev. D **86**, 091101 (2012).
[29] S. Chatrchyan *et al.* (CMS Collaboration), Phys. Lett. B **722**, 207 (2013).
[30] S. Schael *et al.* (ALEPH and DELPHI and L3 and OPAL and LEP Working Group for Higgs Boson Searches Collaborations), Eur. Phys. J. C **47**, 547 (2006).
[31] V. M. Abazov *et al.* (D0 Collaboration), Phys. Rev. Lett. **101**, 071804 (2008).
[32] T. Aaltonen *et al.* (CDF Collaboration), Phys. Rev. Lett. **103**, 201801 (2009).
[33] V. M. Abazov *et al.* (D0 Collaboration), Phys. Lett. B **710**, 569 (2012).
[34] S. Chatrchyan *et al.* (CMS Collaboration), Phys. Lett. B **713**, 68 (2012).
[35] G. Aad *et al.* (ATLAS Collaboration), J. High Energy Phys. 02 (2013) 095.
[36] G. Aad *et al.* (ATLAS Collaboration), J. High Energy Phys. 11 (2014) 056.
[37] CMS Collaboration, Report No. CMS-PAS-HIG-13-025.
[38] J. M. Butterworth, A. R. Davison, M. Rubin, and G. P. Salam, Phys. Rev. Lett. **100**, 242001 (2008).
[39] J. M. Butterworth, A. R. Davison, M. Rubin, and G. P. Salam, arXiv:0810.0409.
[40] M. Carena, P. Draper, S. Heinemeyer, T. Liu, C. E. M. Wagner, and G. Weiglein, Phys. Rev. D **83**, 055007 (2011).

[41] S. Yang and Q. S. Yan, J. High Energy Phys. 02 (2012) 074.
[42] Z. Kang, J. Li, T. Li, D. Liu, and J. Shu, Phys. Rev. D **88**, 015006 (2013).
[43] T. Plehn, G. P. Salam, and M. Spannowsky, Phys. Rev. Lett. **104**, 111801 (2010).
[44] R. Godbole, D. J. Miller, K. Mohan, and C. D. White, Phys. Lett. B **730**, 275 (2014).
[45] R. M. Godbole, D. J. Miller, K. A. Mohan, and C. D. White, arXiv:1409.5449.
[46] Y. L. Dokshitzer, G. D. Leder, S. Moretti, and B. R. Webber, J. High Energy Phys. 08 (1997) 001.
[47] M. Wobisch and T. Wengler, in Monte Carlo Generators for HERA Physics: Proceedings of the workshop 1998-1999.
[48] V. Barger, L. L. Everett, H. E. Logan, and G. Shaughnessy, Phys. Rev. D **88**, 115003 (2013).
[49] A. Djouadi, Phys. Rep. **457**, 1 (2008).
[50] A. Djouadi, Phys. Rep. **459**, 1 (2008).
[51] R. V. Harlander, S. Liebler, and H. Mantler, Comput. Phys. Commun. **184**, 1605 (2013).
[52] D. Eriksson, J. Rathsman, and O. Stal, Comput. Phys. Commun. **181**, 189 (2010).
[53] ATLAS Collaboration, Report No. ATLAS-CONF-2013-079.
[54] V. Ahrens, A. Ferroglia, M. Neubert, B. D. Pecjak, and L. L. Yang, Phys. Lett. B **703**, 135 (2011).
[55] F. Febres Cordero, L. Reina, and D. Wackeroth, Phys. Rev. D **80**, 034015 (2009).
[56] S. Dittmaier *et al.* (LHC Higgs Cross Section Working Group Collaboration), arXiv:1101.0593.
[57] J. M. Campbell, R. K. Ellis, and C. Williams, J. High Energy Phys. 07 (2011) 018.
[58] ATLAS Collaboration, Report No. ATLAS-CONF-2012-097.
[59] ATLAS Collaboration, Report No. ATLAS-CONF-2012-040.
[60] N. D. Christensen and C. Duhr, Comput. Phys. Commun. **180**, 1614 (2009).
[61] J. Alwall, R. Frederix, S. Frixione, V. Hirschi, F. Maltoni, O. Mattelaer, H.-S. Shao, T. Stelzer, P. Torrielli, and M. Zaro, J. High Energy Phys. 07 (2014) 079.
[62] T. Sjostrand, S. Mrenna, and P. Z. Skands, J. High Energy Phys. 05 (2006) 026.
[63] J. de Favereau, C. Delaere, P. Demin, A. Giammanco, V. Lematre, A. Mertens, and M. Selvaggi, J. High Energy Phys. 02 (2014) 057.
[64] M. Cacciari, G. P. Salam, and G. Soyez, Eur. Phys. J. C **72**, 1896 (2012).